Characterization of Weda Bay nickel laterite ore from Indonesia

Saeed Farrokhpay[a,*], Michel Cathelineau[a], Simon B. Blancher[b], Odile Laugier[b], Lev Filippov[a]

[a] Université de Lorraine, CNRS, CREGU, GeoRessources Laboratory, UMR 7359 CNRS, 2 rue du Doyen Marcel Roubault, TSA 70605, 54518 Vandoeuvre-lès-Nancy, France
[b] ERAMET RESEARCH, 1 Avenue Albert Einstein, 78190 Trappes, France

ABSTRACT

The association of fine grained Mg−Ni silicates with oxy-hydroxides in laterites and saprolites represents challenges for ore processing, in particular, in nickel enrichment. The Weda Bay nickel deposit in Indonesia is a typical example of these complex ores, where clays such as nontronites develop on polyphase serpentinite as protolith. Thus, ores at Weda Bay have a very fine textured and complex mineralogy, which requires a comprehensive mineralogical identification through the use of a series of different types of analytical approaches (i.e. macroscopic and microscopic methods including SEM equipped with energy dispersive X-ray spectrometry (EDS), Raman spectroscopy, Infrared and X-ray fluorescence spectroscopy, and QEMSCAN® mapping). Nickel rich saprolites were found to be principally composed of several types of Mg−Ni serpentines, quartz, clays (nontronite in particular) and little amounts of iron hydroxides. Besides, some parts of the deposit were characterized by the development of nontronites at the interface between the saprolite and the limonite zone. Above this zone, the limonite zone is dominated by iron hydroxides as expected, which replace all earlier silicates including serpentine, and contains a significant amount of nickel. The representative composite ore sample contains several nickel bearers with variable nickel grade of 2 to 3%. Exceptionally richer phases such as polygonal Fe (Ni)-rich serpentine were also found with nickel grade of 5 to 10%. Serpentine types as well as other newly formed silicates such as Fe-Mg-(Ni) smectites, are intimately mixed, preventing any mineral separation. Therefore, the only phases which can be separated are quartz and magnetite. This complicates the upgrading of nickel in Weda Bay laterite ore.

1. Introduction

Nickel is an important metal with a total global consumption of about 2 million tons per year which has grown rapidly since the 1940s (Mackey, 2011). About 70% of the nickel resources are present in laterites and the other 30% are in nickel sulphides. It should be noted that these days nickel laterites are more attractive for production of nickel, as the amount of high-grade nickel sulphide ores has been diminished (Janwong, 2012). In addition, the lower cost of exploration of more surficial laterite ores makes these ores more interesting than the deeper set sulphides. However, the challenge of processing nickel laterite ores exists, in particular processing of very fine grained ores with nickel concentration close to the cutting grades. This encourages finding methods that may enhance ore grades which are frequently around the boundary of exploitability (Farrokhpay et al., 2018; Farrokhpay and Fillipov, 2016; Quast et al., 2015).

During lateritization, ultramafic rocks (peridotite) which are more or less serpentinized during their exhumation, are in contact with meteoric waters (Webster and Mann, 1984). The subsequent water-rock interaction yield the dissolution of Mg-silicates, a pH decrease, and the accumulation of the less soluble elements, e.g. iron, as Fe-oxy-hydroxides (Golightly, 2010; Myagkiy et al., 2017). The weathering occurs in sub-tropical climates and provokes leaching of nickel ions and recirculation at elevated pH's (Ashcroft, 2014). The pattern of lateritization highly depends on the drainage, morphology, cementation and climatic changes (Butt and Cluzel, 2013; Golightly, 1981; Skarpelis, 2006). It should be noted that nickel is often extensively dispersed, because silicates are dissolved and Ni−Mg re-precipitated under new mineralogical forms. The process yields to a high reworking of the initial nickel concentrations especially around the water table zone, and results in a monotonous nickel grade in the bulk of the orebody (Cathelineau et al., 2016).

The Weda Bay deposit is located in the central part of Halmahera Island, in the northern part of the Maluku province in eastern Indonesia (Fig. 1). Weda Bay Ni rich laterites developed on dunite and harzburgite as in all other cases elsewhere in Indonesia, New Caledonia, and
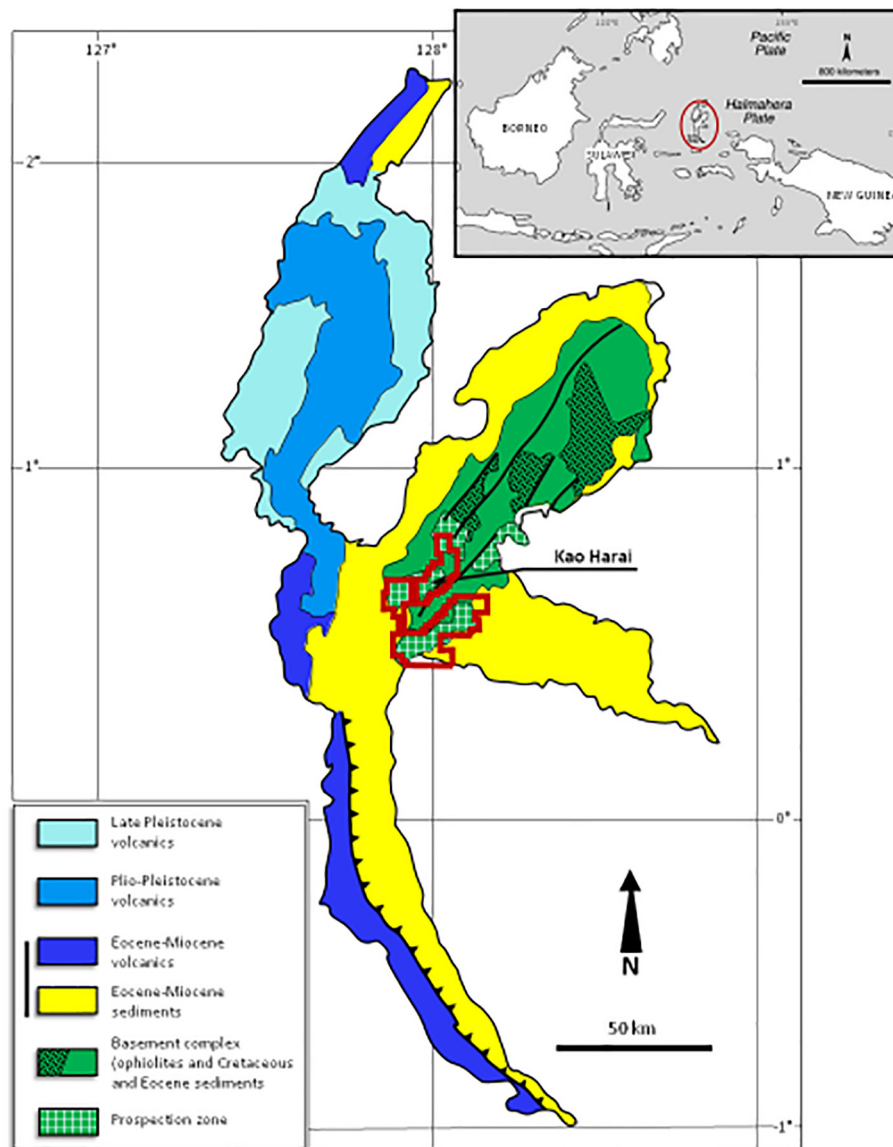

Fig. 1. Simplified geological map of Weda Bay deposit modified after Cock and Lynch (1999).

Australia, during Cenozoic under hot and humid climate. According to Cock and Lynch (1999), the Weda Bay laterite deposits were first drilled in May 1996. Four large laterite areas have been then defined and the reserve evaluation from drillings showed an estimate of about 60 Mt. of 1.5% nickel within an inferred resource of 117 Mt. at 1.3% nickel. The Weda Bay Nickel project was then developed by Eramet since 2009, through a multinational partnership with several companies. Recently, Eramet has announced an agreement with the Chinese Steel Group, Tsingshan, to develop the Weda Bay nickel deposit (ERAMET, 2017). The last estimation of resources mentions 277 million tons at a grade of 1.5% nickel (ERAMET, 2017). This is therefore an area with a potential similar to the giant deposits of Goro (Vale in New Caledonia) or La Sampala (Rio Tinto in Sulawesi) (i.e. deposits with nickel content > 4 Mt).

The correlation between mineralogy, mechanical and textural behaviour of the laterite ores during the ore processing is quite complex (MacCarthy et al., 2015; Quaicoe et al., 2013). A full characterization of different laterite ores is necessary to predict the efficiency of the nickel recovery when different types of ores are blended, which is a common practice in mineral processing industry (Berthomieu et al., 2012). The aim of the present work is therefore to get a full inventory of mineral phases of the Weda Bay laterite ore, and their relative abundances, which are required to predict the exploitability, and to improve the ore processing and nickel upgrading.

1.1. Geology

The Halmahera group belongs to a rather complex geotectonic region where three plates (the Philippine Sea, the Australian and the Eurasian plates) are in contact (Baker and Malaihollo, 1996). The basement of the eastern part of the island consists of a dismembered ophiolitic complex imbricated with slices of Mesozoic and Eocene sediments. The ophiolite complex is overlain unconformably by Middle Oligocene and younger sedimentary and volcanic rocks. The ophiolite complex corresponds to an ocean floor sequence, so-called the Eastern Halmahera-Waigeo province (Sukamto et al., 1981), which extends from central Halmahera to Waigeo Island (in the east). The ophiolites were formed in a supra-subduction zone setting and are considered to be pre-Late Cretaceous in age (Ballantyne, 1991). This age estimate is confirmed by the age of the overlying volcanic and volcanoclastic sequence.

The Weda Bay laterite profile, developed during the Cenozoic, is

Table 1

The Weda Bay profile (adapted from Cock and Lynch, 1999).

	Horizons	Mineralogy	Ni%	Thickness (m)
	Limonite	Goethite Hematite	0.8	2
	Ferruginous saprolite	Ni rich goethite Mn oxides/ hydroxides	1.2-1.6	4-8
	Transition zone			
	Saprolite	Mg silicates Ni rich serpentine Talc, smectite	1.5-2.5	2-4
	Lower saprolite	Ni rich serpentine	0.5-0;8	
	Bedrock	Serpentine Olivine, pyroxene	0.3	

Table 2

Assays of different size fractions (microns) of the laterite ore sample (in wt%).

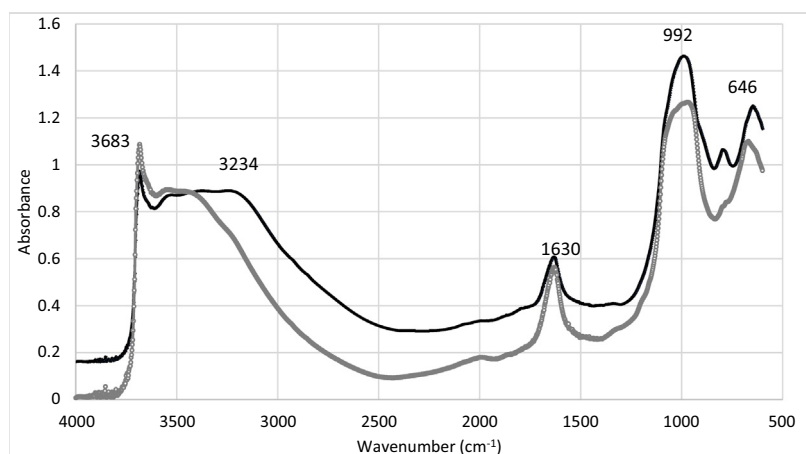| Size	> 4000	4000	1000–4000	1000–350	350–150	150–36	< 36	Bulk (un-sized)
Ni	3.2	3.3	3.2	3.1	2.7	2.1	2.1	2.5
Fe	7.8	9.7	10.4	13.4	19.7	26.3	31.7	28.9
Co	0.2	0.3	0.5	0.5	0.2	0.1	0.1	0.2
Mn	0.1	0.2	0.5	1.8	2.2	1.2	0.8	0.5
Cr	0.3	0.5	0.7	1.6	3.8	2.5	0.5	0.5

Fig. 2. FTIR spectra of the Weda Bay laterite ore sample (black: earthy, and gray: rocky parts).

about 10 m thick, of which 8 m is mineralised with grades in excess of 1% Ni. The profile displays the general layered characteristics of tropical laterites elsewhere. However, the ferricrete capping common to many tropical laterites has been removed by erosion leaving only relict ironstone cobbles and, more commonly, small pisolites that are incorporated into the upper part of the profile (Cock and Lynch, 1999). Below the overburden horizon, a limonite occurs with > 55% Fe_2O_3 and no relics with the pristine textures of the ultrabasic rocks still in place. A certain amount of recognizable grains (quartz, altered serpentine clasts, manganese oxides) are visible within a matrix, brown-

Table 3
A summary of the FTIR peaks assignments (see Fig.7 and the text).

Peak (cm^{-1})	Description	Reference
3683	Stretching vibrations of outer hydroxyl groups coordinated to magnesium of the octahedral layer	(Mellini et al., 2002, Foresti et al., 2009, Liu et al., 2010)
3622	Inner hydroxyl groups coordinated to cations in the octahedral layer with at least one of Mg^{2+} replaced by Fe^{2+} or Ni^{2+}	(Fuchs et al., 1998)
3522, 3400	OH bonded the trivalent cations (such as Fe^{3+} or Al^{3+})	(Serna et al., 1979, Sufriadin et al., 2011)
1630	Banding mode of H−O−H vibration of water molecules	(Motlagh et al., 2011)
992	Stretching vibrations of Si−O−Si bonds	(Tartaj et al., 2000, Foresti et al., 2009)
646	Banding mode of HO−Mg^{2+}	(Zhang et al., 1997)
796	Elongation group of AlO, SiO or MgO bands	

red in colour, dominated by iron oxy-hydroxides. At the basis of this horizon, a transition zone (ferruginous saprolite) is found, and is characterized by more abundant clasts of saprolite within the fine grained goethite matrix (ferruginous saprolite, 25 to 50% Fe$_2$O$_3$ (Cock and Lynch, 1999). Below the ferruginous saprolite, a saprolite horizon (hydrous Mg silicate zone) is characterized by a non-ferruginous texture (< 15% Fe$_2$O$_3$), is green-brown in colour and may be rather soft. The lower saprolite horizon contains fresher green serpentinite and clasts of bedrock.

The profile of the Weda Bay is presented in Table 1.

2. Material and experimental methods

Sampling: The Kao Rahai area, which is the subject of this study is located in what is referred as Central Province in the map from Cock and Lynch (1999), and it corresponds to potential zones in the extension of the project. Representative samples from Kao Rahai area were used for this study. An ore sample (5 kg) containing both a fine iron hydroxide dominated fraction from the ferruginous saprolite, and rocky saprolite blocks from the saprolite horizon was investigated. In order to obtain representative samples, each 1 m fraction sample was first crushed down to 10–20 mm. Then the solids were gathered meter by meter to form the 4 m samples. The blended ore was homogenised and finally sub sampled using riffle splitters.

2.1. Bulk geochemical analysis

X-ray fluorescence (XRF): A portable XLT3 Niton XRF analyser was used for nickel analysis of the different fractions during the processing. XRF is generally used for elemental analysis in solid samples. Since it is fast and easy to use, it is the preferred method for chemical assays. The XRF was calibrated using Atomic Adsorption analysis data. Each element has a different energy level at which their photoelectrons are ejected. Therefore, the intensity of each peak of the resulting spectrum is associated with the quantity of a certain element.

Optical and electron microscopy: In order to establish the mineral paragenesis, firstly the samples were carefully examined with optical microscopy using a transmitted and reflected light microscope. Then SEM analyses were carried out on the polished thin-sections with a JEOL SEM, equipped with an energy dispersive spectrometer using a Si (Li) semi-conductor detector at SCMEM (Nancy, France). The representative areas of the different minerals thus identified were analysed semi-quantitatively by EDS.

Raman spectroscopy: The nature of the serpentine polymorphs, and other silicates was determined on the same areas by Raman spectroscopy performed on the rock sample, as well as on thin and polished sections. The Raman spectra were recorded using a LabRAM HR spectrometer (Horiba Jobin Yvon). The acquisition was performed using a grating of 1800 lines/mm, a slit width of 50 μm and a confocal hole of 500 μm providing a spectral resolution of 0.5 to 1 cm^{-1}. The excitation beam was provided by an Ar$^+$ laser (Stabilite, Spectra Physics, Newport Corporation) at 514.53 nm and a power of 200 mW focused on the

sample using a 50× objective. The spot size was < 1 μm. Acquisition time, limited by a weak luminescence, ranged between 2 s and 6 s. The number of accumulations was set between 10 and 30 to optimize the signal-to-noise ratio within a reasonable acquisition time.

All Mg−Ni hydrous silicates were analysed in two regions of Raman spectroscopy, the low wavenumber (100–1200 cm^{-1}), and the high wavenumber region (3550–3750 cm^{-1}). The main discriminating bands are those corresponding to the OH stretching within the high frequency region. In the region of OH stretching vibrations, the four serpentine polymorphs are distinguished (Auzende et al., 2004; Lemaire, 2000), as well as the talc-like minerals (kerolite-pimelite series) (Cathelineau et al., 2015): i) serpentines: the OH stretching bands for lizardite are at ~3690 cm^{-1} and ~3706 cm^{-1}, for polygonal serpentine at ~3690 cm^{-1} and ~3698 cm^{-1} (Baronnet and Devouard, 1996), for chrysotile at ~3689 cm^{-1} and ~3701 cm^{-1}, and finally for antigorite, two main bands at ~3661 cm^{-1} and ~3698 cm^{-1}, ii) talc: the major OH stretching band is around 3675 cm^{-1}, and iii) talc-like (kerolite-pimelite series): the shape of the OH stretching vibration band shows a strong evolution with increasing nickel content (Cathelineau et al., 2015).

DRIFT measurements: Diffuse reflectance (DRIFT) spectra are recorded with a 2 cm^{-1} spectral resolution using a Fourier transform infrared spectrometer (BRUKER IFS 55) equipped with a large-band mercury cadmium telluride (MCT) detector cooled at 77 ˚K and associated with a diffuse reflectance attachment (Harrick Corporation). Sample preparation involves mixing 50 mg of sample with 320 mg of KBr (potassium bromide). The absorbance unit used corresponds to the decimal logarithm of the ratio R$_{KBr}$/R$_s$ with R$_{KBr}$ the reflectance of the finely powdered KBr used as a reference, and R$_S$ the reflectance of the sample preparation. Each sample is scanned 200 times (90 s) and the influence of atmospheric water was always subtracted.

Microprobe: The EPMA apparatus used in this study was a CAMECA SX100 at ERAMET Research (Trappes, France). Column conditions used were 15 kV and 20 nA. Standards used were apatite (Ca), chromite (Cr), nickel (Ni), hematite (Fe), albite (Na), olivine (Mg), alumina (Al) and quartz (Si). The detection limit was fixed to be around 0.1 wt% on oxides.

2.2. Micromapping using micro-XRF

The latest generation of μ-XRF instrument, the M4 Tornado produced by Bruker-Nano was used to map the main chemical elements of mineral phases studied in thin section. This system has a Rh X-ray tube with a Be side window and poly capillary optics giving an X-ray beam with a diameter of 25–30 μm on the sample. The X-ray tube was operated at 50 kV and 200 μA. X-rays are detected by a 30 mm^2 xflash® Silicon Drift Detector with an energy resolution of < 135 eV at 250,000 cps. All analyses were carried out at 20 mbar vacuum. Main elements such as Fe, Mn, Ni, Co, Mg, Al, and Si were mapped on areas of about 4 × 6 mm.

QEMSCAN®: This analytical technique is dedicated to measure mineral phase proportions (Andersen et al., 2009; Swierczek et al., 2012).
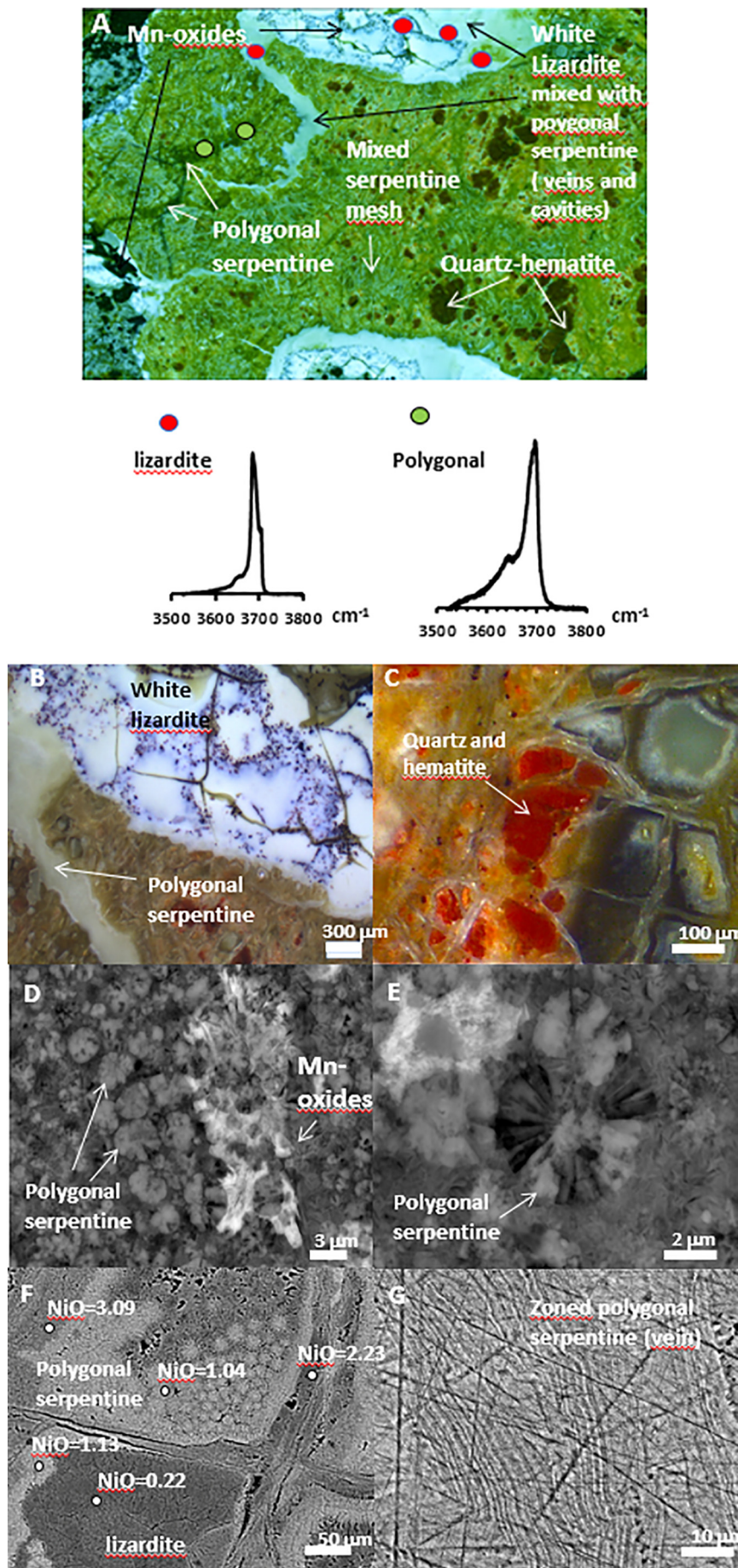
(caption on next page)

Fig. 3. A) Location of the Raman analyses (top image: red and gree dots respresent lizardite and polygonal, respectively), with the corresponding spectra of OH streching (bottom), B) white lizardite and Mn-oxides (black dots), C) pyroxenes replaced by a quartz-haematite assemblage, D, E) polygonal serpentine, F) variations in NiO content of polygonal and white lizardite, G) zoned polygonal infillings in microfracture, (For interpretation of the references to colour in this figure legend, the reader is referred to the web version of this article.)
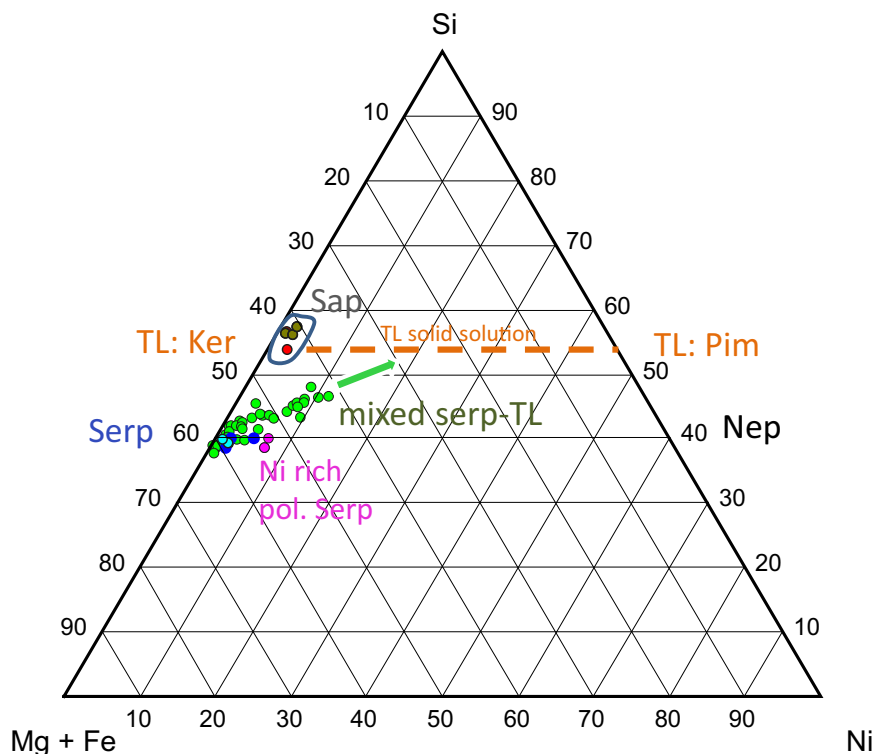

Fig. 4. Si-Mg + Fe-Ni diagram applied to the chemical analyses of serpentines (Serp) as defined from QEMSCAN® images (type 1 to 3) (TL: talk-like, Nep: nepouite, Ker: kerolite, Pim: pimelite).

Table 4
Microprobe analyses of serpentines and smectites in the nickel laterite ore (Fe is assumed as Fe^{+2}).

	Serpentine generation 1			Serpentine generation 2			Serpentine generation 3			Saponite			Stenvensite[a]		
SiO_2	38,2	39,4	35,6	35,71	35,71	38,62	38,98	39,55	41,34	45,82	39,93	45,75	48,63	48,81	50,85
Al_2O_3	0,64	0,64	2,55	< dl	< dl	0,64	1,28	0,64	< dl	0,59	3,55	< dl	1,17	2,35	< dl
MgO	33,6	36,7	33,6	32,22	32,22	31,25	41,56	39,58	41,09	21,15	15,43	19,75	24,63	24,39	24,14
NiO	5,97	2,4	2,39	8,33	8,33	8,31	< dl	2,41	1,21	< dl	2,37	1,20	1,21	2,41	2,40
FeO	2,79	2,85	5,69	2,75	2,75	5,52	< dl	< dl	< dl	5,77	11,32	5,73	< dl	< dl	< dl
CoO	< dl	< dl	< dl	< dl	< dl	< dl	< dl	< dl	< dl	< dl	< dl	< dl	< dl	< dl	1,14
MnO	< dl	< dl	< dl	< dl	< dl	< dl	< dl	< dl	< dl	< dl	< dl	< dl	< dl	< dl	< dl
Total	81,1	81,9	79,8	79,02	79,02	84,34	81,83	82,18	83,63	73,32	72,61	72,43	75,64	77,96	78,54
Si	1,97	1,97	1,85	1,93	1,93	1,95	1,92	1,96	2,00	3,83	3,51	3,90	3,90	3,83	3,98
Al	0,04	0,04	0,16			0,04	0,07	0,04		0,06	0,37		0,11	0,22	
SUM tet	2,01	2,01	2,00	1,93	1,93	1,99	1,99	2,00	2,00	3,89	3,87	3,90	4,01	4,05	3,98
Mg	2,58	2,73	2,60	2,59	2,59	2,35	3,05	2,92	2,96	2,64	2,02	2,51	2,95	2,85	2,82
Ni	0,25	0,10	0,10	0,36	0,36	0,34		0,10	0,05		0,17	0,08	0,08	0,15	0,15
Fe	0,12	0,12	0,25	0,12	0,12	0,23				0,40	0,83	0,41			
SUM oct	2,95	2,95	2,95	3,08	3,08	2,92	3,05	3,02	3,01	3,04	3,02	3,00	3,02	3,01	3,04

[a]) Structural formulae of this mineral show no charges on the octahedral layer, very rich in Mg (about 3%), which is rare in saponite analyses. XRD patterns on oriented thin sections showed a possible small peak at 1.51 A, which is consistent with stenvensite.

It allows mineral identification and classification by using the Energy Dispersive X-ray (EDX) spectra in combination with BSE (Back-Scattered Electron) values of minerals. The QEMSCAN® has been used for lateritic nickel ores where very fine grained (< 1 μm) clay minerals, texturally associated with serpentine and iron hydroxides, once the minerals were previously determined using situ techniques. QEMSCAN® analysis was conducted at Eramet Research using a FEI Quanta 650F SEM (Scanning Electron Microscope) platform with two Bruker Xflash 30 mm silicon drift energy dispersive X-ray detectors. The software used included iMeasure v. 5.2 for the data acquisition and iDiscover v. 5.2 for the spectral interpretation and data processing. The PMA measurement mode was used to collect X-ray data every 2.5 μm across the polished sample surfaces, with X-rays acquired at a total of 2000 X-ray counts per spectrum. The mineral quantifications were calculated by means of surficial proportions of each mineral and their assumed densities.
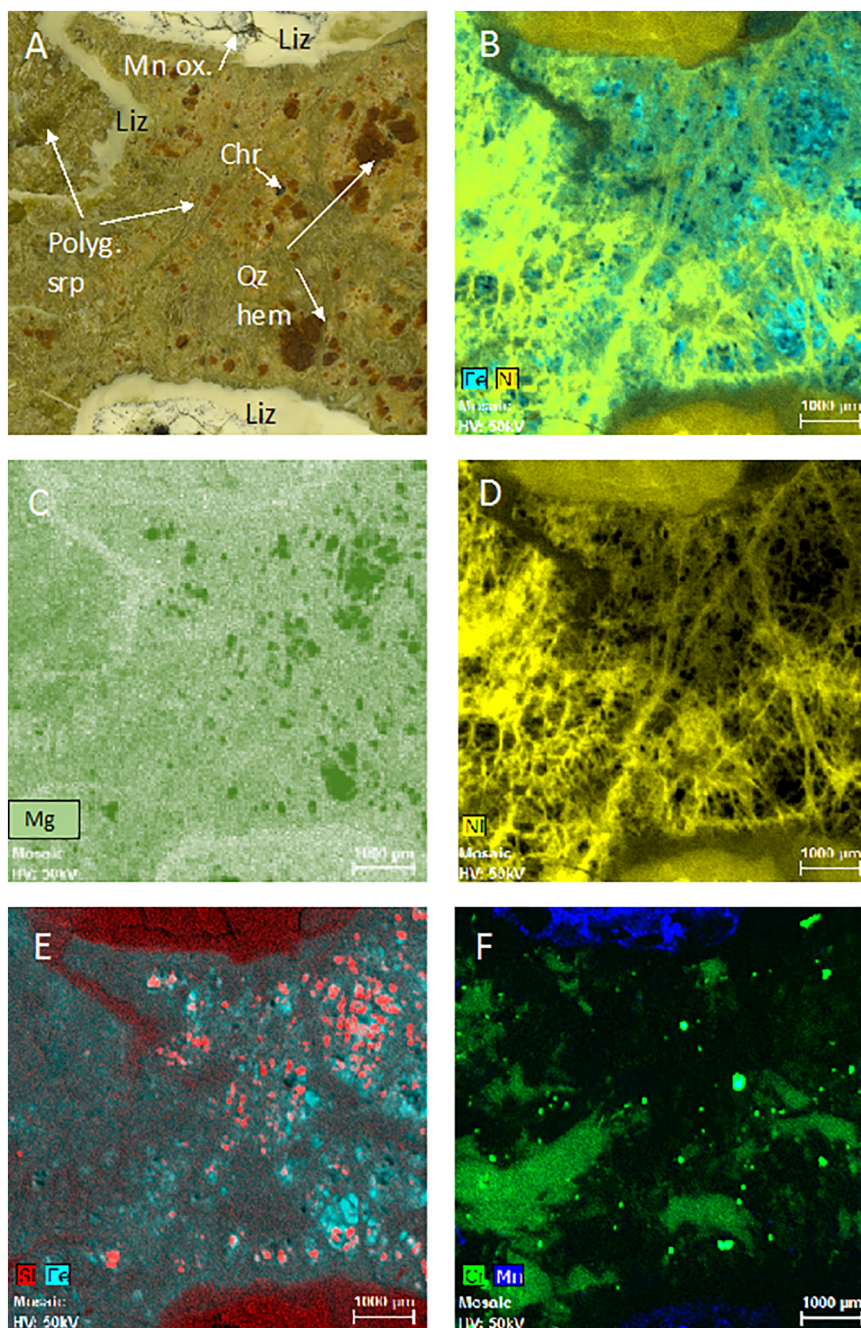
Fig. 5. X-ray microfluorescence maps obtained on the same sample than that presented in Fig. 3.

2.3. Ore processing

Magnetic Separation: Magnetic separation was performed using a modified Jones Wet high intensity magnetic separator (WHIMS). WHIMS is often used for separation of paramagnetic minerals, weakly magnetic materials such as hematite and goethite in the beneficiation of iron ores, iron oxides and ferro silicates from quartz and clays used in manufacturing glass, ceramics and glazes, ilmenite, wolframite and chromite from gangue during concentration, and ferro-oxides and ferro-titanium oxides from cassiterite, zircon and rutile concentrate. A background field intensity of from 15,000 to 20,000 gauss could be achieved in this type of separators. Slurry feed is introduced into the magnetic matrix, which is contained in a stainless steel ring moving at controlled speed between the poles of the powerful stationary electromagnets. Exceptional performance on even weakly magnetic materials,

high magnetic field intensity, middling splitter setting are the key feature of WHIMS (Das and Roy, 2007). Wet separators are normally used to separate strongly magnetic material in finely ground mixture, with the water medium holding the small particles apart for individual action by the magnetic field (Ilschner et al., 1991).

The sample prepared consists of 100 g of < 300 μm (from wet sieving) suspended in 1 L of water (10% solid pulp). The current of 2 A and 10 A makes the magnetic field equivalent to 0.1 and 0.6 T, respectively. Therefore, 2 A separation aims ferromagnetic and 10 A separation aims paramagnetic minerals. After installing the matrix between the solenoids, the water flow and pulp flow was adjusted to 2 L/min and 6 L/min, respectively. Then, the cycle was set to start at 2 A. The second separation was carried out at 10 A.

Size classification: The laterite ore sample was classified using wet sieving. Sieves at 36, 80, 150, 300 μm, and 1 and 4 mm were used for
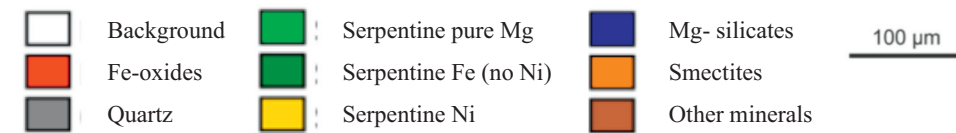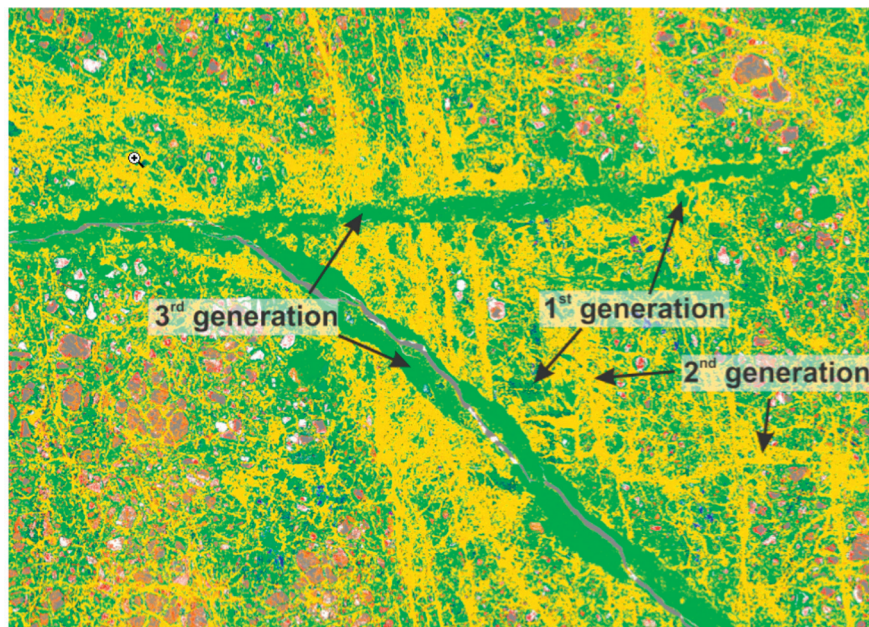
Fig. 6. QEMSCAN® mineralogical mapping of the ore sample showing three generations of serpentine.
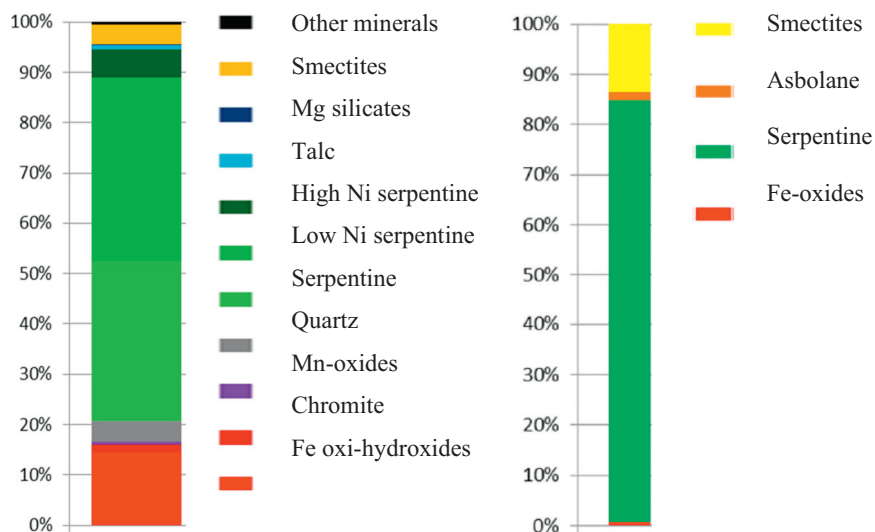

Fig. 7. QEMSCAN® modal mineralogy (left) and nickel deportment (right) of the laterite ore sample.

this purpose. Ore particles at different size fractions were filtered, dried and chemically assayed. The minus 300 μm size fraction was used for the ore processing tests.

3. Results and discussion

3.1. Bulk rock characterization

Analysis of the unsized (bulk) sample shows that the ore contains 2.5% and 28.9% Ni and Fe, respectively. The other minor elements were measured at 0.2% Co, 0.5% Mn and 0.5% Cr (Table 2).

The nickel concentration was found in between 2.1 and 3.3 wt% in the different size fractions as illustrated in Table 2. The rocky saprolite blocks are richer in nickel than the fine grained fractions that are enriched in iron oxi-hydroxides. It should be noted that the nickel grade in laterites is often poorly associated with the major elements (Ilyas et al., 2016).

Fig. 2 shows the DRIFT spectra of both rocky saprolite and fine fraction. The sharp peak at 3683 cm^{-1} is attributed to the stretching vibrations of outer hydroxyl groups coordinated to the magnesium of the octahedral layer (Foresti et al., 2009; Liu et al., 2010; Mellini et al., 2002), which shows the presence of serpentine in the sample. The 3622 cm^{-1} band is associated with inner hydroxyl groups coordinated to cations in the octahedral layer, in which at least one of the Mg^{2+} has
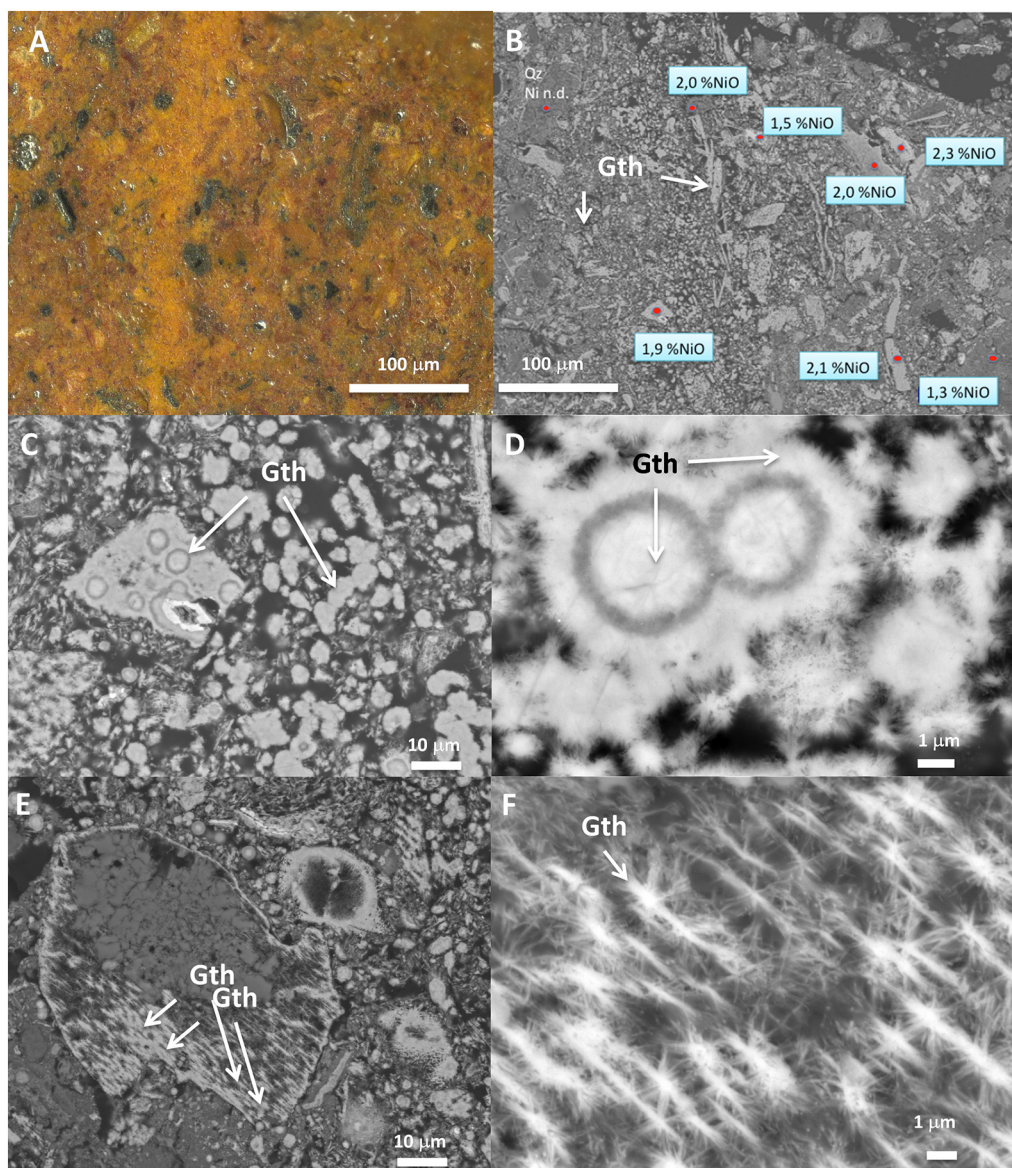
Fig. 8. Main features of the fine grained part of the representative ore sample dominated by earthy saprolite: A: macroscopic feature of the earthy saprolite (fine fraction) sample, B: distribution of NiO concentration in the same sample, C: detailed texture of goethite replacemet textures, D: magnfication of goethite spherolites, E: location of goethite onto the border, cleavages of former pyroxenes, F: detail of goethite needles developed in the same grain.

been replaced by Fe^{2+} or Ni^{2+} (Fuchs et al., 1998). The peak at $3522\,cm^{-1}$ and the broad peak at about $3400\,cm^{-1}$ are due to the OH bonded the trivalent cations (such as Fe^{3+} or Al^{3+}), as well as Mg-rich smectites (e.g. saponite) (Serna et al., 1979; Sufriadin et al., 2011), which shows the presence of smectite, as well as possibly Fe and Al hydroxides. The sharp peak around $1630\,cm^{-1}$ is due to the banding mode of the H−O−H vibration of water molecules (Motlagh et al., 2011), which can be corresponded by the H_2O in the smectites interlayers. The other sharp peak at $992\,cm^{-1}$ is attributed to the stretching vibrations of Si−O−Si bonds (Foresti et al., 2009; Sufriadin et al., 2011; Tartaj et al., 2000) and the peak at around $646\,cm^{-1}$ is due to the banding mode of HO−Mg^{2+} (Zhang et al., 1997) with more particularly from the external O−H bands (Sontevska et al., 2007). The assignments for major FTIR peaks are summarized in Table 3.

3.2. Mineral assemblages and in situ characterization of main mineral phases

Serpentinized protolith and rocky saprolite: Several textures of serpentine polymorphs were identified by petrology analysis (Fig. 3): i) classic "mesh" texture which corresponds to the typical early replacement of olivine and pyroxene by a mixture of antigorite and lizardite (Fig. 3A, upper part), ii) infillings of fractures or micro domains by white lizardite (Fig. 3A, upper part and Fig. 3B) as shown by the Raman OH stretching bands at $3690\,cm^{-1}$ and $3705\,cm^{-1}$ (Fig. 3a lower part), and iii) a network of thin veinlets of greenish serpentine, characterized by typical OH bonds of polygonal serpentine identified by Raman spectroscopy at $3689\,cm^{-1}$ and $3700\,cm^{-1}$ and typical textures (Fig. 3C and D). Ghosts of pyroxene porphyroblasts are entirely replaced by quartz and Fe hydroxides (Fig. 3C). The whitish domains dominated by the newly formed lizardite and by relics of polygonal serpentine (Fig. 3B and F) host in addition Mn oxides/hydroxides containing high concentration of nickel. The NiO contents are highly heterogenous at small scale, as shown by Fig. 3F where NiO contents range from 0.20% to 3.09% depending on the nature of the serpentine. The white serpentine has NiO concentrations ranging from 0.2% to 5.8% and the polygonal serpentine (green in color, and chemically zoned, Fig. 3G) has NiO concentration of 3.0% to 9.5%. Mn oxides/
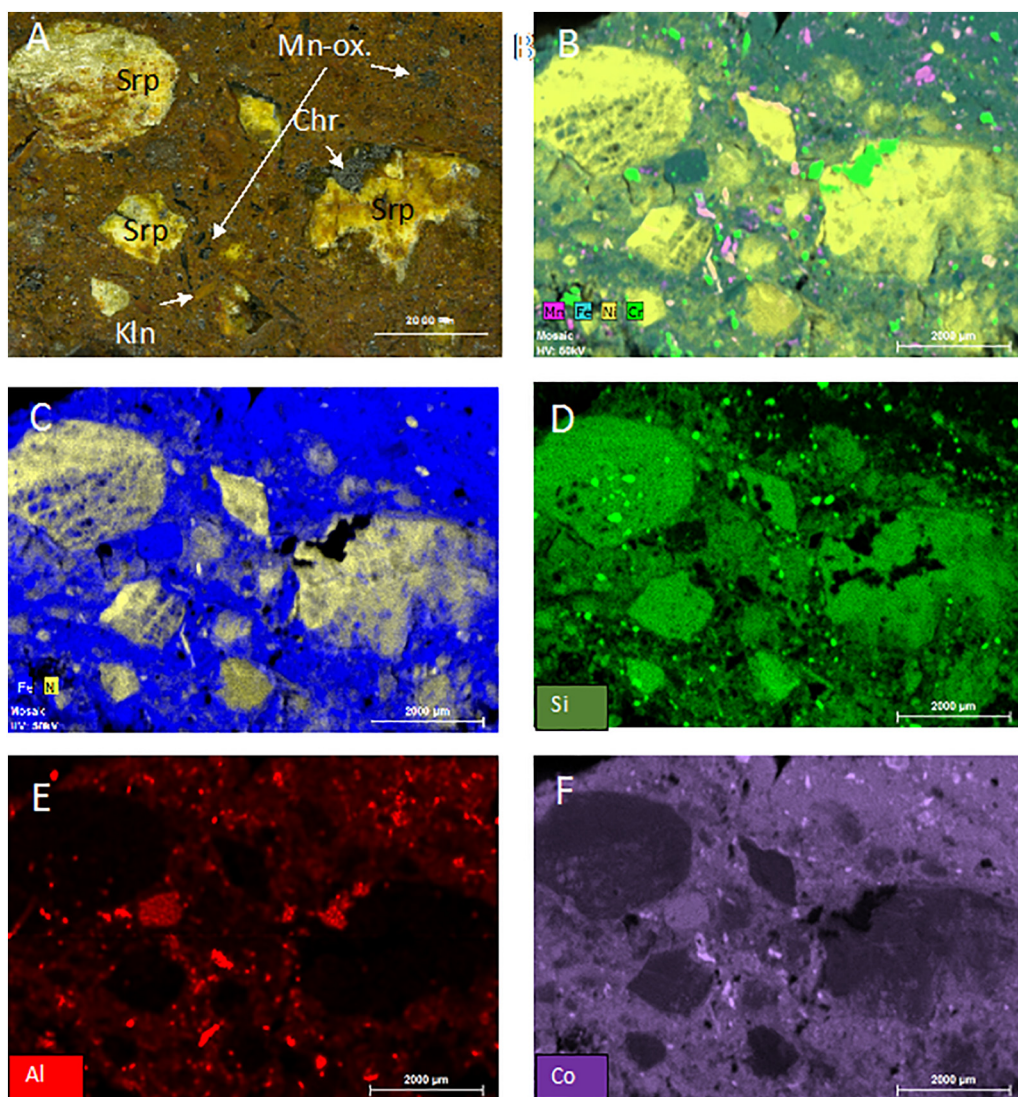
Fig. 9. A: microphotograph of the mapped area with micro-XRF; B: composite image of Mn, Fe, Ni and Cr images showing the distribution of chrmoite relics (green) and manganese oxides rich in Co (magenta); C: Composite image of Ni and Fe showing that Ni is mostly within the relics of serpentinized fraction, and within Fe-oxihydroxides; D: Si distribution showing local spots of quartz grains, E: Al distribution showing local Al concetrations linked to Al hydroxydes, F: Co distribution showing its highest concentration in Mn oxides, and within the Fe-oxihydroxides. (For interpretation of the references to colour in this figure legend, the reader is referred to the web version of this article.)

hydroxides are as usual rich in Ni, which ranges from 18% to 24% NiO, and form clusters of grains.

The SEM-EDX microanalysis data (Fig. 4) revealed that more nickel is incorporated in the greenish polygonal type serpentines, compared to the white lizardite, and a stoichiometric deviation in direction to nickel-talc like (pimelite end-member) is observed. This trend is similar to the data reported by Villanova-de-Benavent et al. (2014) and by Fritsch et al. (2016) for the Dominican Republic and New Caledonia laterites, respectively. The results may be interpreted as the development of talc-like phases at the expense of serpentine, which results in analyses plotting in between the two end-members.

In the earthy saprolite, above the rock saprolite, several clay minerals have been determined: nontronite, iron-saponite and stevensite, which are three different smectites. Structural formulae determined from microprobe analyses confirm the identification of these minerals (Table 4). Structural formulae are calculated on 7 and 11 oxygens for serpentine and smectites, respectively, and mean values reported in Fig. 4.

X-Ray Microfluorescence maps: Fig. 5 shows the X-ray micro-fluorescence maps of the same sample as previously analysed by Raman spectroscopy (Fig. 3). The maps reveal that nickel is mostly linked to the network of micro-fractures sealed by the green polygonal serpentine. The fact that part of the network is enriched in nickel and other depleted could indicate that this distribution is linked to a secondary nickel enrichment. The parts of the rock bearing the lowest nickel concentration are the silicified, hematite bearing phenocrysts of pyroxene relics, and the earlier interstitial serpentine outside the network of polygonal serpentine. Chromite is distributed as small grains dispersed within the matrix, and Mn-oxides are present as patches in particular within the white lizardite.

QEMSCAN® map: QEMSCAN® mineralogical mapping of the sample block (Fig. 6) shows the succession of three generations of serpentine: 1) Fe-rich and Ni-poor growing directly at the expense of pre-existing Mg-silicates 2) Mg-rich and Ni-rich, along the polygonal serpentine micro-fracture network, and 3) Mg-rich and Ni-poor, which represents the last phase of serpentine crystallization (white lizardite), which is located in fissures with quartz.

Fig. 7 also shows that Ni-enrichment is not linked with the first stage of serpentinization. The first generation of serpentine probably appears during an intense metasomatic process (Golightly, 1981). Then, the weathering of this serpentinite and the formation of the lateritic profile leads to Ni, Mg and Si leaching in the upper part of the profile, and to their recrystallization in the lower one. Ore definition and resources estimations are therefore dependent on the amount of the second generation of serpentine and on its liberation. The leaching of the limonite layer is progressive, with two big steps: the first with the removal of nickel and iron, and the second with the destabilization of Mg-silicates.
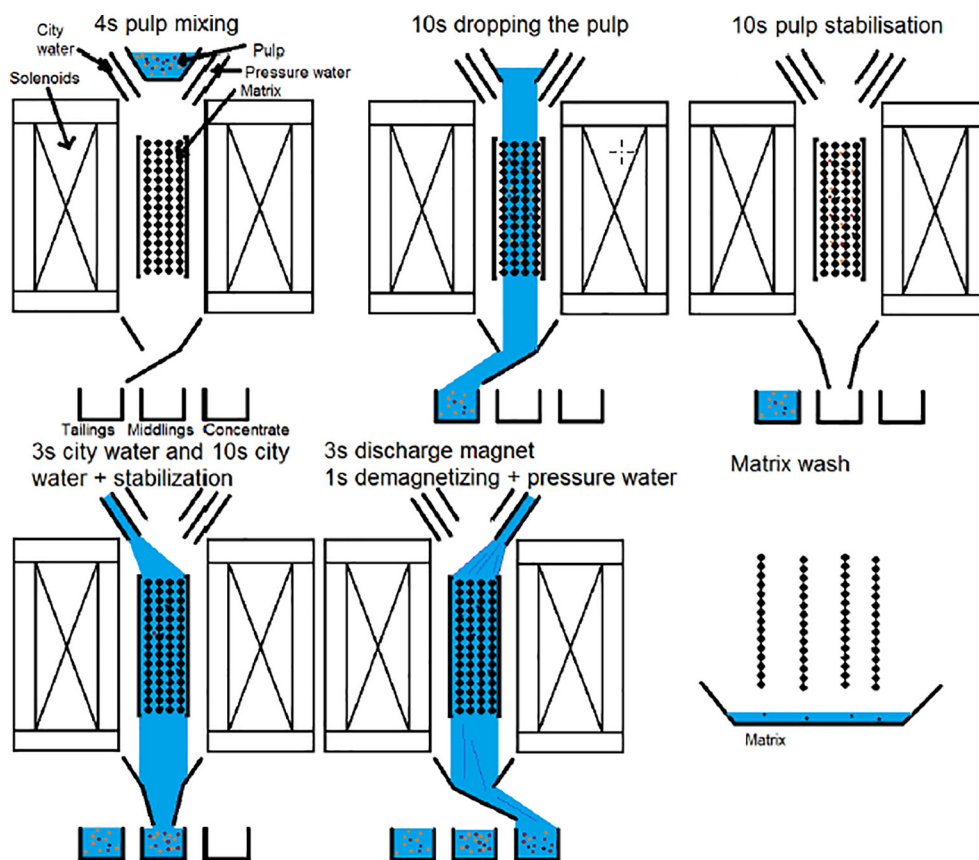
Fig. 10. A schematic diagram of the magnetic separation cycle used in the current work.

3.3. Earthy saprolite (fine fraction)

Mineral textures: Most mineral phases observed in the rocky saprolite are replaced by goethite (Fig. 8A). Goethite forms thus a great part of the fine earthy saprolite fraction. The NiO content measured by WDS-SEM analysis of each grain ranges from 1.0% to 2.5%, with a mode around 1.5–2.0% NiO, in good agreement with the mean values of bulk rocks in this horizon (Fig. 8B). The linear grains correspond to the replacement by goethite or to crystallization of goethite onto earlier structures such as cleavage planes, or the external envelope of minerals. In open spaces, goethite develops as dispersed radiated spherolites composed of thin elongated crystals (Fig. 8C and D). When the mineral shapes are still intact and not collapsed, the mineral volume appear empty (Fig. 8E). The cleavages, such as those of the pyroxenes, appear underlined by the development of very fine needles of goethite, which form stars aligned along the cleavage (Fig. 8F). The average length of the needle-shaped goethite crystals is from 1 to few microns.

Fig. 9 also shows the X-ray micro-fluorescence maps of the same sample as previously analysed by Raman spectroscopy (Fig. 8). The maps reveal that nickel occurs mostly within the relics of the serpentinized fraction, and within Fe oxy/hydroxides.

3.4. Ore processing

A schematic diagram of the Cycle of magnetic separation used in the current work is shown in Fig. 10. It was found that the Weda Bay laterite ore has about 8% magnetic part (magnetite, Fe_3O_4) with no (or very minimal) nickel content. The result of SEM and EDS analysis revealed that the ferro-magnetic part of the ore sample contains 97.3% FeO. The remaining contains MgO (1.7%), SiO_2 (0.3%) and TiO_2 (0.7%). These data suggest that magnetic separation may be useful in pre-concentrating nickel from the Weda Bay laterite ore (if economically feasible). It should be noted that the amount of the magnetic fraction has been reported to increase with decreasing pulp density, since at a low pulp density the particles are better dispersed and therefore are exposed to the magnetic field (Kim et al., 2010).

4. Conclusions

Three different serpentines as Fe-rich/Ni-poor, Mg-rich/Ni-rich, and Mg-rich/Ni-poor were identified quantitatively on the QEMSCAN images. They correspond to two distinct polytypes: lizardite and polygonal serpentine. The green polygonal serpentine network in the saprolite horizon is the best enriched in nickel. Above, in the weathered serpentinite, a local development of clays, especially nontronites is observed.

As the three types of serpentines have similar behaviour during physical separation, it is almost impossible to separate them and to enrich the nickel grade of the ore. Quartz and the chromite/magnetite/hematite fraction are the only phases that can be separated, but they represent a small amount of the ore of the ore. Magnetic separation may however be useful in the pre-concentration stages.

In conclusions, this study shows the usefulness of combined multi-technique mineral determinations together with two complementary methods of chemical imaging: micro-XRF and EDS. The Weda Bay composite sample is a typical example of a nickel laterite with features, which will be even more common in future nickel mining activities. More work is needed to investigate if increasing the amount of separable magnetic fraction is possible, and if the nickel silicate fraction can be separated or at least enriched, in the range of fractions of nickel percent. Therefore, the very complex distribution of nickel among silicates having similar properties, and the mixing of silicates and iron hydroxides still remains the main challenge.

Acknowledgements

References

Andersen, J.C.Ø., Rollinson, G.K., Snook, B., Herrington, R., Fairhurst, R.J., 2009. Use of QEMSCAN® for the characterization of Ni-rich and Ni-poor goethite in laterite ores. Miner. Eng. 22, 1119–1129.

Ashcroft, G., 2014. Nickel Laterites: The World's Largest Source of Nickel. https://www.geologyforinvestors.com/nickel-laterites/.

Auzende, A., Daniel, I., Reynard, B., Lemaire, C., Guyot, F., 2004. High-pressure behaviour of serpentine minerals: a Raman spectroscopic study. Phys. Chem. Miner. 31, 269–277.

Baker, S., Malaihollo, J.A.F., 1996. Dating of neogene igneous rocks in the Halmahera region: arc initiation and development. Geol. Soc. Lond. Spec. Publ. 106, 499–509.

Ballantyne, P.D., 1991. Petrological Constraints upon the Provenance and Genesis of the East Halmahera Ophiolite. Orogenesis in Action. Journal of South East Asian Earth Science, pp. 259–269.

Baronnet, A., Devouard, B., 1996. Topology and crystal growth of natural chrysotile and polygonal serpentine. J. Cryst. Growth 166, 952–960.

Berthomieu, B., Dissaux, A., Le Quesne, Y., 2012. Recovery of Nickel and Cobalt from the Weda Bay Lateritic Deposit (Halmahera, Indonesia) Using an Atmospheric Leaching Process, ALTA Nickel-Cobalt-Copper Conference. pp. 96–112.

Butt, C.R.M., Cluzel, D., 2013. Nickel laterite ore deposits: weathered serpentinites. Elements 9, 123–128.

Cathelineau, M., Caumon, M.C., Massei, F., Brie, D., Harlaux, M., 2015. Raman spectra of Ni–Mg kerolite: effect of Ni–Mg substitution on O–H stretching vibrations. J. Raman Spectrosc. 46, 33–940.

Cathelineau, M., Quesnel, B., Gautier, P., Boulvais, P., Couteau, C., Drouillet, M., 2016. Nickel dispersion and enrichment at the bottom of the regolith: formation of pimelite target-like ores in rock block joints (Koniambo Ni deposit, New Caledonia). Mineral. Deposita 51, 271–282.

Cock, G.C., Lynch, J.E., 1999. Discovery and Evaluation of the Weda Bay Nickel/Cobalt Deposits Central Halmahera, Indonesia, PACRIM 99 Congress. AusIMM.

Das, A., Roy, S., 2007. Magnetic Separation - Principles and Application in Beneficiation of Iron Ores. Iron Ore, NML, Jamshedpur, pp. 89–102.

ERAMET, 2017. Press Release. http://www.eramet.com/en/press-releases?page=2.

Farrokhpay, S., Fillipov, L., 2016. Challenges in processing nickel laterite ores by flotation. Int. J. Miner. Process. 151, 59–67.

Farrokhpay, S., Fillipov, L., Fornasiero, D., 2018. Upgrading nickel in laterite ores by flotation. Miner. Eng. 121, 100–106.

Foresti, E., Fornero, E., Lesci, I.G., Rinaudo, C., Zuccheri, T., Roveri, N., 2009. Asbestos health hazard: a spectroscopic study of synthetic geoinspired Fe-doped chrysotile. J. Hazard. Mater. 167, 1070–1079.

Fritsch, E., Juillot, F., Dublet, G., Fonteneau, L., Fandeur, D., Martin, E., Caner, L., Auzende, A.-L., Grauby, O., Beaufort, D., 2016. An alternative model for the formation of hydrous Mg/Ni layer silicates ('deweylite'/'garnierite') in faulted peridotites of New Caledonia: I. Texture and mineralogy of a paragenetic succession of silicate infillings. Eur. J. Mineral. 28, 295–311.

Fuchs, Y., Linares, J., Mellini, M., 1998. Mossbauer and infrared spectrometry of lizardite-1T from Monte Fico, Elba. Phys. Chem. Miner. 26, 111–115.

Golightly, J.P., 1981. Nickeliferous Laterite Deposits. Economic Geology, 75th Anniversary Volume. pp. 710–735.

Golightly, J.P., 2010. Progress in Understanding the Evolution of Nickel Laterite. Society Economic Geologist Special Publication 15. pp. 451–485.

Ilschner, B., Grant, N.J., Russell, K.C., 1991. Materials Beneficiation. Springer-Verlag Inc., New York.

Ilyas, A., Kashiwaya, K., Koike, K., 2016. Ni grade distribution in laterite characterized from geostatistics, topography and the paleo-groundwater system in Sorowako, Indonesia. J. Geochem. Explor. 165, 174–188.

Janwong, A., 2012. The Agglomeration of Nickel Laterite Ore. University of Utah.

Kim, J., Dodbiba, G., Tanno, H., Okaya, K., Matsuo, S., Fujita, T., 2010. Calcination of low-grade laterite for concentration of Ni by magnetic separation. Miner. Eng. 23, 282–288.

Lemaire, C., 2000. Application des spectroscopies vibrationnelles à la détection d'amiante dans les matériaux et à l'étude des serpentines, 157 pp. Université de Paris 7.

Liu, K., Chen, Q.Y., Hu, H.P., Yin, Z.L., 2010. Characterization and leaching behavior of lizardite in Yunjiang laterite ore. Appl. Clay Sci. 47, 311–316.

MacCarthy, J., Nosrati, A., Skinner, W., Addai-Mensah, J., 2015. Effect of mineralogy and temperature on atmospheric acid leaching and rheological behaviour of model oxide and clay mineral dispersions. Powder Technol. 286, 420–430.

Mackey, P., 2011. Nickel Pyrometallurgy Short Course: Introduction to Nickel. Conference of Metallurgists Nickel Pyrometallurgy, Sudbury.

Mellini, M., Fuchs, Y., Viti, C., Lemaire, C., Linares, J., 2002. Insights into the antigorite structure from Mossbauer and FTIR spectroscopies. Eur. J. Mineral. 14, 97–104.

Motlagh, M.M.K., Youzbashi, A.A., Sabaghzadeh, L., 2011. Synthesis and characterization of nickel hydroxide/oxide nano particles by the complexation-precipitation method. Int. J. Phys. Sci. 6, 1471–1476.

Myagkiy, A., Truche, A., Cathelineau, M., Golfier, F., 2017. Revealing the conditions of Ni mineralization in the laterite profiles of New Caledonia: insights from reactive geochemical transport modelling. Chem. Geol. 466, 274–284.

Quaicoe, I., Nosrati, A., Skinner, W., Addai-Mensah, J., 2013. Agglomeration behaviour and product structure of clay and oxide minerals. Chem. Eng. Sci. 98, 40–50.

Quast, K., Connor, J.N., Skinner, W., Robinson, D.J., Li, J., Addai-Mensah, J., 2015. Preconcentration strategies in the processing of nickel laterite ores part 2: laboratory experiments. Miner. Eng. 79, 269–278.

Serna, C.J., White, J.L., Velde, B.D., 1979. The effect of aluminium on the infrared spectra of 7 Å trioctahedral minerals. Mineral. Mag. 43, 141–148.

Skarpelis, N., 2006. Lateritization processes of ultramafic rocks in Cretaceous times: the fossil weathering crusts of mainland Greece. J. Geochem. Explor. 88.

Sontevska, V., Jovanovski, G., Makreski, P., 2007. Mineral from Macedonia part XIX: vibrational spectroscopy as identificational tool for some sheet silicate minerals. J. Mol. Struct. 834, 328-327.

Sufriadin, Idrus, A., Pramumijoyo, S., Warmada, W., Imai, A., 2011. Study of mineralogy and chemistry of the saprolitic nickel ores from Soroako, Sulwesi, Indonesia: implication for the laterite ore processing. J. South East Asia Appl. Geol. 3, 23–33.

Sukamto, R., Apandi, T., Supriatna, S., Yasin, A., 1981. The geology and tectonics of Halmaheraa nd the surroundingis lands. In: Barber, A.J., Wiryosujono, S. (Eds.), The Geology and Tectonics of Eastern Indonesia. Spec. Publ. Geol. Res. Dev. Cent., Bandung, pp. 349–362.

Swierczek, Z., Quast, K., Addai-Mensah, J., Connor, J.N., Robinson, D.J., Li, J., 2012. Challenges in the mineralogical characterisation of low grade nickel laterites. In: XXVI International Mineral Processing Congress (IMPC), New Delhi, pp. 5352–5536.

Tartaj, P., Cerpa, A., García-González, M.T., Serna, C.J., 2000. Surface instability of serpentine in aqueous suspensions. J. Colloid Interface Sci. 23, 176–181.

Villanova-de-Benavent, C., Proenza, J.A., Galí, S., García-Casco, A., Tauler, E., Lewis, J.F., Longo, F., 2014. Garnierites and garnierites: Textures, mineralogy and geochemistry of garnierites in the Falcondo Ni-laterite deposit, Dominican Republic. Ore Geol. Rev. 58, 91–109.

Webster, J.G., Mann, A.W., 1984. The influence of climate, geomorphology and primary geology on the supergene migration of gold and silver. J. Geochem. Explor. 22, 21–42.

Zhang, Q., Sugiyama, K., Saito, F., 1997. Enhancement of acid extraction of magnesium and silicon from serpentine by mechanochemical treatment. Hydrometallurgy 45, 323–331.